A High Dense Temperature-Salinity Dataset Observed by ~~Automatic~~Autonomous Underwater Vehicles toward Mesoscale eddies' Evolutions and Associated Submesoscale Processes in South China Sea

Chunhua Qiu[1,2], Zhenyang Du[1,2], ~~Jiancheng Yu[3], Huabin Mao[4],~~ Haibo Tang[1,2], Zhenhui Yi[1,2], Jiawei Qiao[1,2], Dongxiao Wang[1,2,*] , Xiaoming Zhai[3~~5~~], ~~Yeqiang Shu[4]~~Wenbo Wang[1,2]

1. School of Marine Sciences, State Key Laboratory of Environmental Adaptability for Industrial Products, Sun Yat-Sen University, and Southern Marine Science and Engineering Guangdong Laboratory (Zhuhai), Zhuhai, China

2. Guangdong Provincial Key Laboratory of Marine Resources and Coastal Engineering, School of Marine Sciences, Sun Yat-sen University, Guangzhou 510275, China

~~3. State Key Laboratory of Robotics, Shenyang Institute of Automation, Chinese Academy of Sciences, Shenyang 110016, China~~

~~4. State Key Laboratory of Tropical Oceanography, South China Sea Institute of Oceanology, Chinese Academy of Sciences, Guangzhou, China~~

~~5~~3. Centre for Ocean and Atmospheric Sciences, School of Environmental Sciences, University of East Anglia, Norwich, UK

Corresponding author:

Dongxiao Wang

School of Marine Sciences,

Sun Yat-sen University

Email: dxwang@mail.sysu.edu.cn

Abstract. Marginal seas are usually fulfilled with strongly varying mesoscale eddies (MEs), which evolutions plays vital roles in regulating global oceanic energy equilibrium, triggering subemesoscale processes with strong vertical velocity, and inducing high biogeochemistry transport. But the temporal evolutions of MEs and submesoscale processes with several kilometers' resolutions are difficult to be measured by traditional observations with passive working mode. The ~~automatic~~ underwater gliders (~~AUG~~UGs) and vehicles (AUVs) positively observe oceanic motion, and could provide us spatiotemporal synchronization information for strongly varying MEs. Here, we present a 9-year high dense dataset of AUVs/~~AUG~~UGs observations in 2014-2022 in the South China Sea (SCS) can be downloaded from https://doi.org/10.57760/sciencedb.11996 (Qiu et al., 2024b). Totally, 9 ~~AUG~~UG and 2 AUV cruise experiments were conducted, and 50 ~~AUG~~UGs (2 AUVs) equipment were deployed with zonal and temporal resolutions of < 7 km and <6 hour. It covers the area of eddy's birth, propagation, and dissipation, presenting us the most complete data to investigate the evolution of MEs at different life stages. 40% of them reach resolutions < 1 km and < 1 hour, which provides us the dynamic characteristics of submesoscale instabilities across and along front at the eddy edge. This dataset has potential in improving the forecast accuracy in physical and biogeochemistry numerical model. Much more aggressive field investigation programs will be promoted by the NSFC in future.

Keywords: ~~Automatic~~Autonomous Underwater Vehicles; Mesoscale eddies; submesoscale processes; South China Sea

1. Background

Evolutions of mesoscale eddies (MEs), with high geostrophic straining, favors the generation of submesoscale processes with several kilometers' spatial resolution (McWilliam, 2016), and requires high-accuracy, spatiotemporal synchronization and dense observations. Marginal seas (such as, Gulf of Mexico, South China Sea, Mediterranean) are usually fulfilled with ~~multi-scale oceanic motions, i.e. boundary current, mesoscale eddie~~MEs (~~MEs;~~ Rossby number $R_o = U/fL \approx 0.1$), and smaller scale processes ($R_o > 1$). MEs, with spatial scale of 50–300 km and temporal scale of several weeks to months, play vital roles in the transport of matter and energy (Chelton et al., 2007; Morrow et al., 2004). They are numerous in the global ocean and also in the tropical marginal sea of South China Sea (SCS; Chen et al., 2011; Wang et al., 2003; Xiu et al., 2010). They easily generate by obtaining kinetic energy from large-scale current, and easily dissipate to submeso- or smaller- scale processes at the slope region via shear and baroclinic instabilities (Oey, 1995; Okkonen et al., 2003).

Observation plats for MEs include ship-cruise, satellite, Argo float, mooring, drifters, ~~automatic~~autonomous unmanned vehicle (AUV), and ~~automatic~~ underwater gliders (~~AUG~~UG), etc. These plats have been utilized to detect variations of MEs in SCS (Table 1). Ship-cruise observations are the most traditional methods to investigate the MEs' general structures (Wang et al., 1987; Xu et al., ~~1996~~1997), but difficult to track their spatiotemporal evolutions. Satellite data provide wide surface information of MEs (i.e., temporal and spatial scales; Chelton et al., 2011) and air-sea interactions have been revealed (Ni et al., 2021). Southwest of Taiwan Islands, northwest of Luzon Islands, Xisha Islands region, and east of Vietnam are the four main eddy birth pools (Hwang et al., 2000; Wang et al., 2003; Nan et al., 2011). After birth, MEs move westward, southwestward, or northwestward under the control of the first-baroclinic Rossby wave (Lin et al., 2007; Xiu et al., 2010; Chen et al., 2011). Since 2002, a large number of Argos have been deployed, providing routine measurements to describe vertical structures of MEs (He et al., 2018; Table 1). The spatiotemporal resolutions of Argo profiles are approximately 100 km and 10 days, which is difficult to capture the high-frequency variability of MEs and submesoscale processes (Table 1).

Table 1. Observation studies of ME in SCS.
ME: mesoscale eddies; SCS: South China Sea

Ship Observation (CTD Station)	Dale, 1956	Cool pool near Vietnam
	Wang et al., 1987	Warm eddy near southwestern of Taiwan Islands
	Xu et al., ~~1996~~1997;	Northwest of Luzon Islands, named Luzon cold eddy
	Li et al., 1998	A warm eddy in northeast of NSCS
	Chu et al., 1998	An eddy pair in central of SCS.
	Fang et al., 2002	Vietnam warm eddy
Satellite Observations (sea level anomaly; velocity)	Hwang et al., 2000; Wang et al., 2003; Nan et al., 2011~~a~~	Topex/Poseidon altimeter data, 94 cold eddy, 124 warm eddy. Southwest of Taiwan Islands, northwest of Luzon Islands, East of Vietnam.
	Lin et al., 2007; Chen et al., 2011; Xiu et al., 2010	Radius, life cycle, tracking, seasonal and interannual variations of mesoscale eddies
	He et al., 2016	The role of ENSO on interannual variation in Luzon Strait mesoscale eddies
	He et al., 2019	MEs' influence on Chl-a
Argo; Mooring	Li et al., 2022	Vertical tilt of Mesoscale eddy
	He et al., 2018	Reconstruction data combine altimeter and Argos, revisit the three-dimensional structures of ME
	Zhang et al., 2017	By using mooring array, investigate eddy looping from Luzon Strait

Attributed to the positively track, AUVs and ~~AUG~~UGs become more and more important tools in exploring marine environment over last two decades, due to the advantages of low cost, long-duration, controllability and reusability. Our group has collected dense UGs and AUVs observations across MEs. UGs adjust buoyancy to generate gliding motion through water columns by a pair of wings, and hybrid underwater gliders have been developed since 2004 (Bachmayer et al., 2004; Caffaz et al., 2010). Many international products of ~~AUG~~UGs were operated, such as "Seaglider" (Eriksen et al., 2001), "Spray" (Sherman et al., 2001), "Slocum" (Webb et al., 2001), "Deepglider" (Osse and Eriksen, 2007), "SeaExplorer". ~~Their~~ UGs' product companies and related information are listed in Table 2. UGs moves in a sawtooth trajectory at a slow speed of 0.3 m/s, while AUVs are propeller-driven, acting as sawtooth and drifting mode at the maximum speed of 1 m/s (Hobson et al., 2012). It takes around 8/3 days for a UG/AUV to pass a quasi-steady eddy with mean radius of ME (100 km) in SCS. Kinds of sensors, such as, conductivity-temperature-depth(CTD), GPS are installed on the UGs and AUVs to measure marine environment. Hence, ~~Multi-year AUG~~UGs and AUVs have been successfully used in detecting strongly varying features in some marginal seas, such as estimation of trends of Gulf Stream (Todd and Ren, 2023), the water mass exchanges between Bay of Bengal and Arabian Sea (Rainville et al., 2022). We reported ~~AUG~~UGs experiments since 2014 (Qiu et al., 2015), and made AUV experiments since 2018 (Huang et al., 2019; Qiu et al., 2020). Here, we present 9-year (2014-2022) AUVs and ~~AUG~~UGs datasets in SCS, and try to show their potential abilities in detecting the evolutions of MEs and the associated submesoscale processes.

Table 2. Types of several popular UGs (underwater gliders)

Types	Development Organizations
Seaglider	University of Washington
Spray	Scripps Institute of Oceanography and Woods Hole, https://spray.ucsd.edu/pub/rel/info/spray_description.php
Slocum serials	Webb Research Cor.
Deepglider / Oculus	Kongsberg Underwater Technology, Inc.
SeaExplorer glider	ACSA, Sep.5, 2013 https://www.marinetechnologynews.com/news/seaexplorer-underwater-glider-record-487228
Sea Wing	Shenyang Institute of Automation, Chinese Academy f Sciences https://baike.baidu.com/item/%E6%B0%B4%E4%B8%8B%E6%BB%91%E7%BF%94%E6%9C%BA/4560334
Petrel	Tianjin University; https://baike.baidu.com/item/%E2%80%9C%E6%B5%B7%E7%87%95%E2%80%9D%E5%8F%B7%E6%B0%B4%E4%B8%8B%E6%BB%91%E7%BF%94%E6%9C%BA/13977071

2. Data Description

2.1 ~~AUG~~UG and AUV experiment sites

Different with Rainville et al (2022) and Todd and Ren (2023), most of our experiments aimed to detect the evolution of MEs or submesoscale processes. Two products of Chinese ~~AUG~~UGs named “Sea Wing” and “Petrel” are utilized in revealing the development of MEs in this study. Since 2014, we have conducted 11 experiments, totally collecting 24498 temperature and salinity profiles, which is even more than those in Gulf Stream (Todd and Ren, 2023). 50 ~~AUG~~UGs and 2 AUVs were deployed in northern SCS. The deploying time, installed sensors, and diving depths of ~~AUG~~UGs/AUVs experiment were shown in Table 3. More detailed information, including vehicle serial number, waypoints, matching time, latitude, and longitude is stored in the data with *.NC format. The gray highlighted the ~~AUG~~UG network experiments, with number of ~~AUG~~UGs ≥3. Such as, in the experiments of 2017, 2019 and 2020, more than 10 ~~AUG~~UGs were deployed to detect the three-dimensional structures of the mesoscale eddies. The largest ~~AUG~~UG network was conducted in 2021, including 50 ~~AUG~~UGs, which was set to investigate eddy-current interaction.

Table 3. Information of individual ~~AUG~~UG/AUV experiment and the observing purpose. ME: Mesoscale Eddies; AUV: Autonomous Underwater Vehicle; UG: Underwater Glider.

Number	Equipment	Time	Number of Qualified Profiles	Number of Eliminated Profiles (Stage)	Number of equipment	Sensor of equipment (*: with Shipped CTD~~; ##: with DO and Chl-a sensors; ++: Velocity~~)	Diving depth of equipment	Observing Purpose
1	~~AUG~~UG	Sept. 19- Oct. 15, 2014; 26 days	227	0	1 ~~AUG~~UG	Seabird Glider Payload CTD(GPCTD)	1000 m	Mixed layer heat budget; sea trials
2	~~AUG~~UG	Apr. 18-Jul. 6, 2015; 78 days	~~446~~1359	0	3 ~~AUG~~UGs Network	Seabird Glider Payload CTD(GPCTD)	1000 m	Structures of ME
3	~~AUG~~UG	Jul. 14-~~Aug~~UG. 13, 2017 30 days	~~3016~~2998	3(Syntax Test)	10 ~~AUG~~UGs, Network	Seabird Glider Payload CTD(GPCTD)~~; Aanderaa oxygen optode probes and WETLabs fluorescent probes ##~~	300 m (3) 1000 m (7)	ME response to TC
4	~~AUG~~UG	Apr. 22-May 23, 2018; 31 days	239	0	1 ~~AUG~~UG, Virtual mooring	Seabird Glider Payload CTD(GPCTD)	1000 m	Structures of ME
5	~~AUG~~UG	Jul. 13- Sept. 30, 2019; 77 days	~~15840~~3707	3(Syntax Test)	~~50~~ 17 ~~AUG~~UGs, Network	Seabird Glider Payload CTD(GPCTD) *	~~300 m (4)~~ 1000 m (17~~42~~) ~~4500 m (4)~~	Slope intrusion of ME
6	AUV	Sept. 18- Oct. 23, 2019; 35 days	~~143~~131	5(Gross Range Test)	1 AUV	SBE37 CTD; DVL++	300 m	Evolution of ME
7	~~AUG~~UG	Jun. 26- ~~Aug~~UG. 27, 2020; 60 days	~~3515~~3365	14(Location Test& Syntax Test)	12 ~~AUG~~UGs	Seabird Glider Payload CTD(GPCTD)	1000 m	Slope current
8	~~AUG~~UG	Jul. 26- ~~Aug~~UG. 8, 2021; 13 days	~~467~~307	8(Syntax Test); 152(Gross Range Test);	2 ~~AUG~~UGs	RBR legato CTD	300 m (1) 1000 m (1)	Edge of ME
9	~~AUG~~UG	~~Aug~~UG. 7- ~~Aug~~UG. 27, 2021; 20 days	~~219~~215	4(Gross Range Test);	2 ~~AUG~~UGs	Seabird Glider Payload CTD(GPCTD)	1000 m	Edge of ME
10	AUV	May 9- Jul. 29, 2021; 80 days	~~169~~167	2(Gross Range Test);	1 AUV	SBE37 CTD	300 m	Evolution of ME
11	~~AUG~~UG	Jun. 23- Jul. 6, 2022; 13 days	217	0	2 ~~AUG~~UGs	Seabird Glider Payload CTD(GPCTD)	1000 m	Edge of ME
Total	/	463 days	~~24498~~12932	191	~~83~~ 50 ~~AUG~~UGs, 2 AUVs	/	/	Structures and evolution of ME

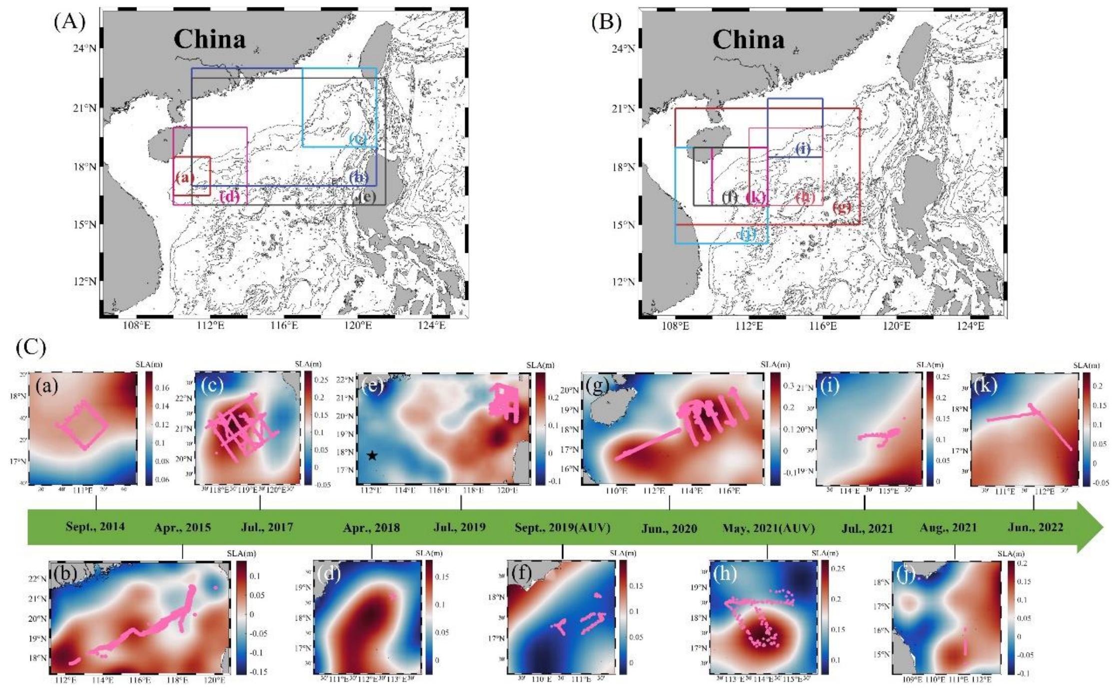

Figure 1. Underwater glider (UG) and autonomous underwater vehicle (AUV) observation sites. (A) observation area for subplots (a)-(e); (B) area for subplots (f)-(j). The grey lines in (A) and (B) are the water depth. (a)-(j) Observation stations (pink dots) with sea level anomaly (SLA, shading colors). The observation times are (a) September, 2014; (b) April, 2015; (c) July, 2017; (d) April, 2018; (e) July, 2019; (f) September, 2019; (g) June, 2020; (h) May, 2021; (i) July, 2021; (j) August, 2021; and (k) June, 2022.

2.2 Intercomparison of ~~AUG~~UGs / AUVs resolution

The ~~AUG~~UGs and AUVs positions with the mean sea level anomalies (SLAs) during experiment time were shown in Figure 1. Note that all the ~~AUG~~UGs and AUVs crossed MEs with positive/negative SLAs. The spatial and temporal resolutions of samples were presented in Figure 2. The dominant spatial resolution (blue bars) was 4-7 km in 2014, 2015, and 2019, while it was less than 3 km in other years. In 2017 (Figure 2c), July 2021 (Figure 2f) and 2022 (Figure 2h), the temporal resolution of ~~AUG~~UGs achieved 1-2 hours, while it was 4-7 hours in other experiments. It indicates that all of the experiments could resolve the MEs (spatial scale of 50-300 km), and 40% of them could be used to resolve submesoscale processes (spatial scale of <3 km).

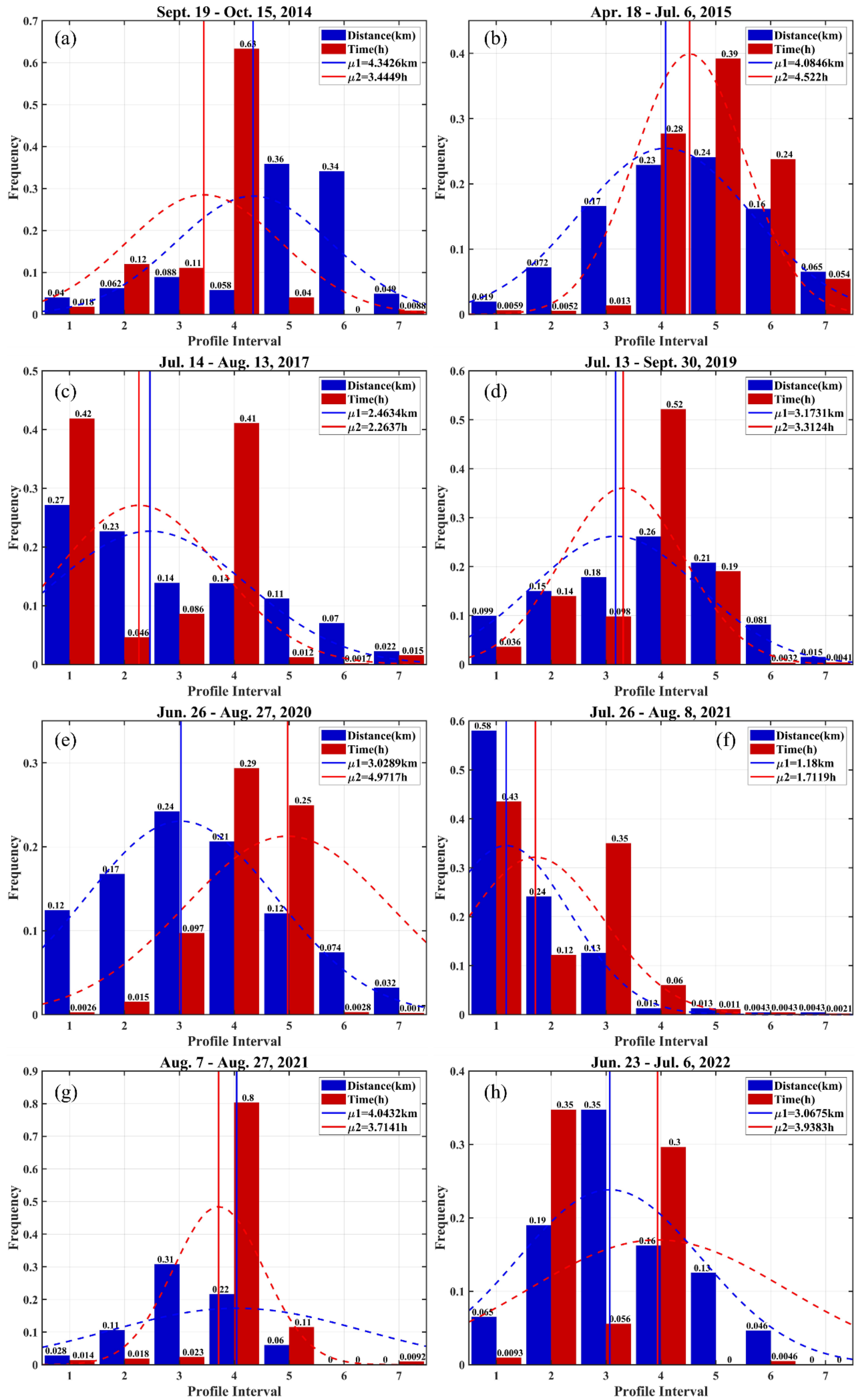

Figure 2. Frequency of spatial (blue bar) and temporal (red bar) sample interval. The red and blue bars (dashed red and blue lines) denote probabilities of spatial and time interval (the normal distributions of spatial and time intervals), respectively.

3 Data Quality Control Method

Before investigating the three-dimensional structures of MEs, we did quality control for the ~~AUG~~UGs and AUVs.

3.1 Quality control for ~~AUG~~UG data

Two products of Chinese ~~AUG~~UGs named "Sea-wing" and "Petrel" were used in this study. The communication and navigation subsystem contain iridium satellite communication devices, wireless communication devices, a precision navigation attitude sensor, a Global Positioning System (GPS) device, a pressure meter, and obstacle avoidance sonar. A conductivity-temperature-depth (CTD) sensor with ~6 s sampling resolutions has been installed on the two ~~AUG~~UG products.

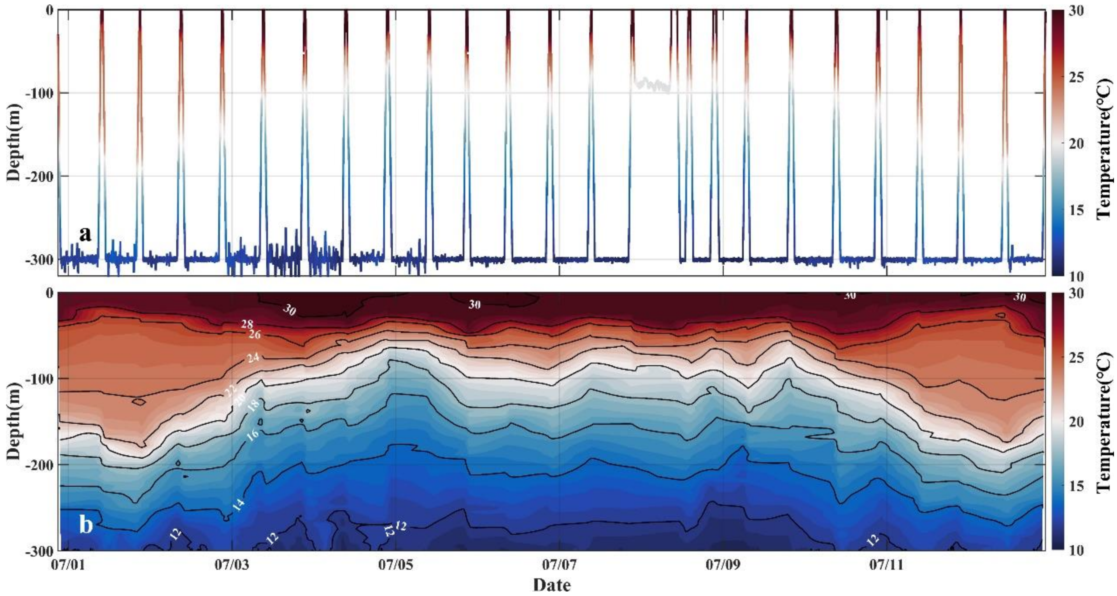

Figure 3. Illustration of (a) original, and (b) interpolated data after quality control. The AUV duration is in July 2021. AUV: autonomous unmanned vehicle.

Before investigating oceanic phenomena, we did data quality control following standard of integrated ocean observing system (IOOS). The quality control for UG (https://repository.oceanbestpractices.org/handle/11329/289?show=full) includes 9 steps: (1) Timing/Gap Test: Test determines that the profile has been received within the expected time window and has the correct time stamp; (2) Syntax Test: Ensures the structural integrity of data messages; (3) Location Test: Test if the reported physical location (latitude and longitude) is within the reasonable range determined by the operator;(4) Gross Range Test: Ensure that the data points do not exceed the minimum/maximum output range of the sensor; (5) Pressure Test: Test if the pressure records increase monotonically with depth, sorted the vertical depth values and removed any duplicate depth values; (6) Climatology Test: Test if the data points are within the seasonal expectation range; (7) Spike Test: Test if the data points exceed the selected threshold compared to adjacent data points, excluded the data with temperature/salinity larger than 35 °C/35 psu; (8) Rate of Change Test: Test if the rate of change in the time series exceeds the threshold determined by the operator; (9) Flat Line Test: Test for continuously repeated observations of the same value, which may be the result of sensor or data collection platform failure. After that a natural neighbored interpolation is utilized to the temperature and salinity to 1-m vertical resolution data.

We have validated the ~~AUG~~UG observed temperature and salinity profiles with ship observed data during July, 2019 (black star in Figure 1e; Figure 4). The mean bias of temperature is 0.05 ℃, and that of salinity is 0.01 psu. The vertical temperature/salinity profiles of ship and ~~AUG~~UG installed CTD are consistent, supporting that the data are credible.

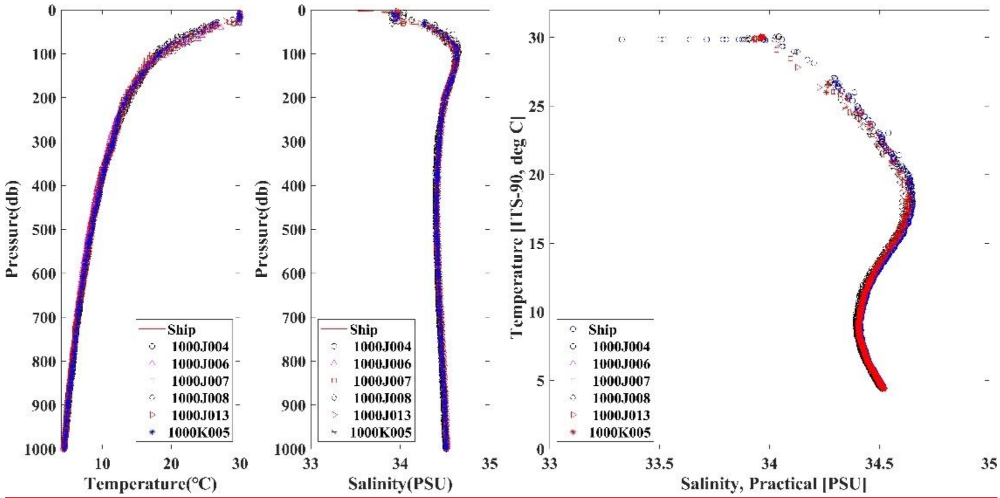

Figure 4. Comparison of (a) temperature, (b)salinity, and (c) temperature-salinity scatter plots between ship installed CTD and AUV installed CTD at station (112.0661°E, 17.7778°N). Red line in (a) and (b) is the ship measured values. Dot, green triangle, red square, diamond, red triangle, and blue star are for UGs named 1000J004, 1000J006, 1000J007, 1000J008, 1000J013 and 1000K005, respectively. ~~Different symbols are the different AUG.~~

3.2 Quality control for AUV data

Both CTD and GPS instrument were installed on the “Sea-Whale 2000” AUV. This AUV was designed by Institute of Shenyang Automation, Chinese Academy of Sciences. It could operate in two modes, a “sawtooth-like” mode and a “cruise” mode at a depth of 300 m (Huang et al., 2019).

In the “sawtooth-like” mode, the data quality control procedures are the same as those for ~~AUG~~UGs. Figures 3 and 4 show the AUV observed temperature after data-quality. In “cruise” mode, the AUV navigates at the depth of around 300 m. Following Qiu et al (2020), we firstly transformed the temperature and salinity at depth z to those at 300 m using a linear regression method ($\mathrm{T}' = 0.008\mathrm{z}' + 0.017; S' = -0.0002z' + 0.0006$),

$$T' = T_z - T_{mean}, \tag{1a}$$

$$S' = S_z - S_{mean}, \tag{1b}$$

where T_{mean} is averaged using a 10-point smooth average, which could maintain the spatial variations from 20 to 30 km. Depth anomaly is defined as the measured depth minus 300 m, $\mathrm{z}' = \mathrm{z} - 300$, and the temperature and salinity anomalies as $\mathrm{T}'$and S', respectively. We compared this method with the potential temperature algorithm, and the temperatures obtained at 300 m were highly consistent.

3.3 Density derived from temperature and salinity

The value of seawater density (ρ, in kg/m^3) can be calculated based on temperature (T in °C), salinity (S in psu), and pressure (P in dbar). The UNESCO formula provides a simplified approach to estimate seawater density as follows:

$$\rho(S,T,P) = \frac{\rho_0(S,T)}{1 - \frac{P}{K(S,T,P)}} \tag{2a}$$

$$\rho_0(S,T) = \rho_{sw}(T) + (b_0 + b_1 T_{68} + b_2 T_{68}^2 + b_3 T_{68}^3 + b_4 T_{68}^4)S + (c_0 + c_1 T_{68} + c_2 T_{68}^2)S\sqrt{S} + d_0 S^2 \tag{2b}$$

$$\rho_{sw}(T) = a_0 + a_1 T_{68} + a_2 T_{68}^2 + a_3 T_{68}^3 + a_4 T_{68}^4 + a_5 T_{68}^5 \tag{2c}$$

$$T_{68} = T \times 1.00024 \tag{2d}$$

where $\mathrm{K(S,T,P)}$ is secant bulk modulus, a_0 and others are coefficients. This formula accounts for the haline and thermal contraction of seawater. The detailed method is related to https://unesdoc.unesco.org/ark:/48223/pf0000188170.

4. Data Application

4.1 Intra-thermocline (Subsurface) MEs observed by AUGUGs and AUVs

Cross-eddy tracks of AUGUG or AUV could observe both the warm core and cold cores (Figure 4). In April 2015, one AUGUG crossed a warm eddy, and observed a subsurface warm core (Figure 1b & Figure 5a). The warm core ranges from 50-500 m depth with radius about 100 km, which is termed as intra-thermocline anticyclone and has been reported in Shu et al (2016). Qiu et al (2019) utilized the same experimental dataset to investigate the asymmetry structures of this intra-thermocline eddies, suggesting that the centrifugal force should be taken into account when revealing the velocity of MEs, i.e. gradient wind theory. This gradient wind theory has been cited in a deriving global cyclogeostrophic currents data (Cao et al. 2023). In June 2020 (Figures 1g & 5d-f), one AUGUG captured a subsurface cold eddy with a negative temperature and positive salinity core, which is the value minus the zonal mean value. And the highly dense core ranged from surface to 500 m depth. Above all, single AUGUG/AUV could capture both the surface and the intra-thermocline eddy's position, range and strength.

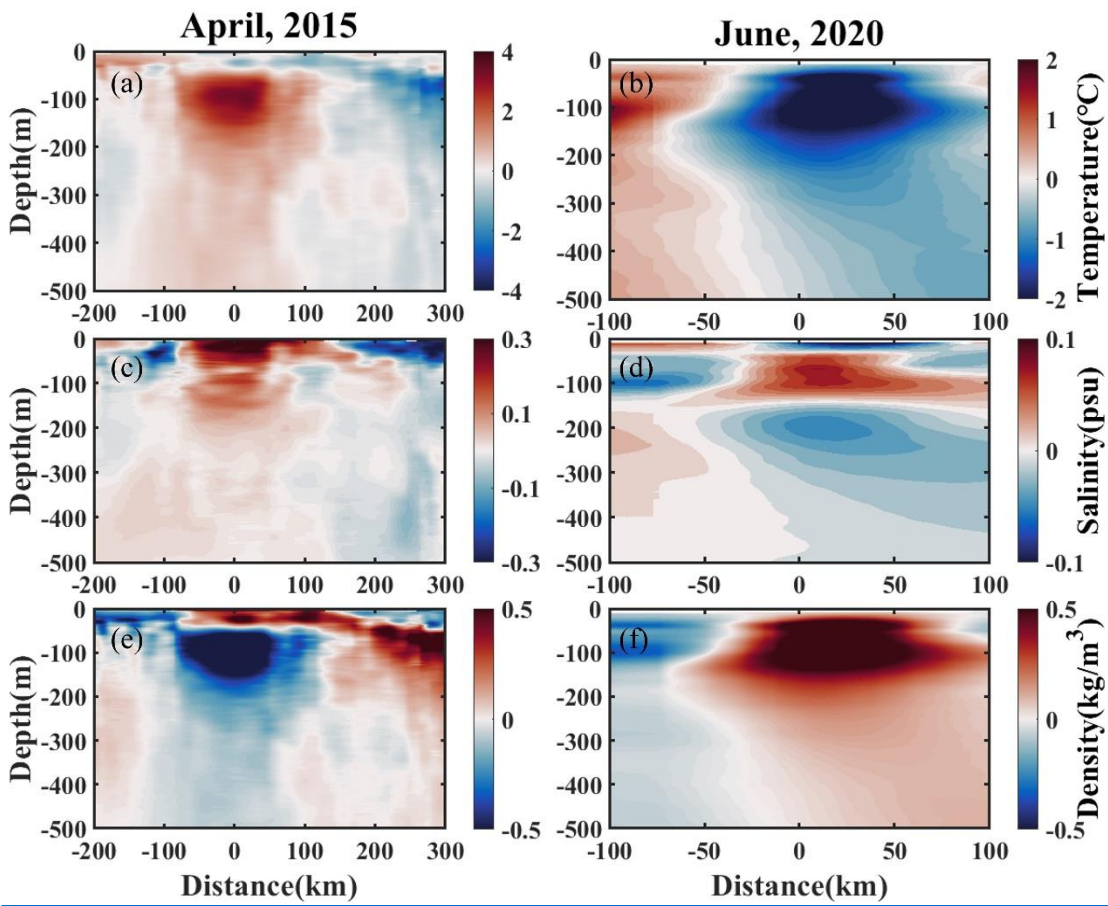

Figure 5. Contour of (a) and (b) temperature anomaly (c) and (d) salinity anomaly, (e) and (f) density anomaly in April, 2015(left panels) and June, 2020(right panels).

~~AUG~~UG/AUV could track the development of intra-thermocline MEs. During developing stage, MEs can easily deform and may cause cross-slope transports at the continental slope (Wang et al., 2018; Su et al., 2020; Qiu et al., 2022), and produce submesoscale process (Dong et al., 2018; Yang et al., 2019). To observe the development of ME, “Sea-Whale 2000” AUV have traversed an anticyclonic ME using 5 repeated rectangular tracks from May to July 2021(Figure 1h). This experiment was supported by National Key R&D Program.

An anti-cyclonic eddy with low Brunt-Väisälä frequency squared value ($N^2 = \frac{1}{\rho}\frac{d\rho}{dz} < 10^{-4}$ s^{-1}), located in the subsurface layer from 50-200 m depth, and existed as an intra-thermocline anticyclonic eddy (Figure 6). The repeated cruise of AUV was separated to five stages, termed as T1(June 8-11), T2 (June 19-23), T3 (June 29- July 4), T4 (July 10- 15), and T5 (July 21-26). Taking 22.5 kg/m^3 and 23.5 kg/m^3 as the upper and lower boundary of the intra-thermocline ME, we calculated the area and the mean temperature within the mesoscale eddy. The area and mean temperature decreased from T1-T3, and then increased from T4-T5, indicating the intra-thermocline anticyclonic eddy weakened from T1-T3 and strengthened from T4-T5. This development has been described in detail by Qiao et al (2023), who found the eddy moved eastward during T1-T3 and got stuck during T4-T5.

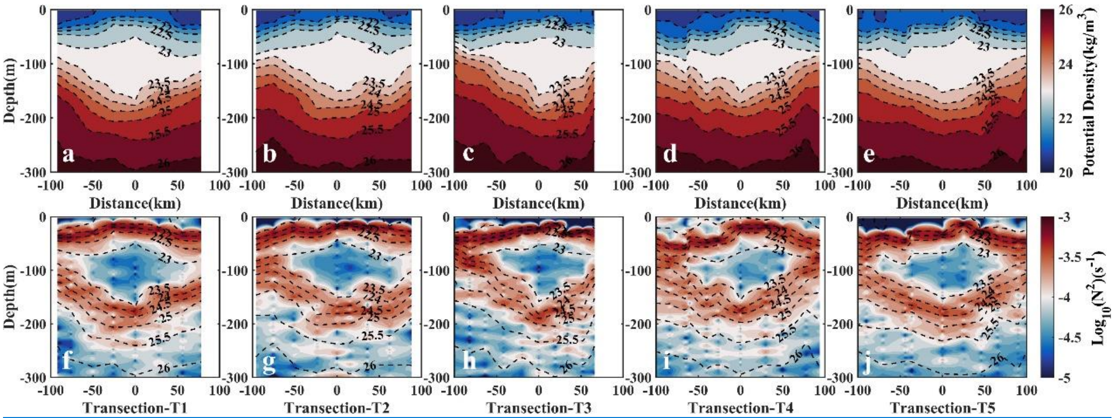

Figure 6. The profiles of density (upper panel) and Brunt frequency (lower panel) during (a,f)T1, (b,g)T2, (c,h)T3, (d, i)T4, (e, j)T5 period, which was 06/08-06/11,06/19-06/23,06/29-07/04,07/10-07/15,07/21-07/26, respectively.

4.2 Vertical Tilt of MEs at different life-stages observed by ~~AUG~~UGs

Several systematic ~~AUG~~UG networks were conducted in 2015, 2017, 2019, and 2020. A whole life cycle of ME usually experiences birth, developing, mature and dissipate stages (Zhang and Qiu, 2018; Yang et al., 2019), and the eddy's age has suggested to influence on the kinetic energy of ME. Luzon strait is an eddy birth zone, where Kuroshio branch intrudes the SCS (Chen et al., 2011; Su et al., 2020). And then, most of the eddies move westward to the continental shelf zone under the modulation of Rossby wave, finally dissipate in Dongsha Islands, Xisha Islands or merged with other eddies (Yang et al., 2019; Su et al., 2020; Qiu et al., 2022).

The systematic ~~AUG~~UG experiments provide us probability in capturing the different vertical structures of MEs at different life stages. After data quality, we firstly mapped the temperature and salinity data onto 1 km × 1 km × 1 m grid, and then calculated the water density, ρ. The ME follows geostrophic balance, that is, the geostrophic velocity could be derived under the force balances between pressure gradient and Coriolis force. Finally, we derived the geostrophic velocity, v_g, by using thermal-wind relationships,

$$v_g(x,y,z) = v_0 - \frac{g}{f\rho_0}\int_{z0}^{z}\left(\frac{\partial\rho(x,y,z)}{\partial x} + \frac{\partial\rho(x,y,z)}{\partial y}\right)dz, \qquad (3)$$

where ρ_0 is the referenced water density, f is the Coriolis frequency, v_0 is the referenced geostrophic velocity at depth 1000 m and assumed to be 0.

Figure 7a-b depicts the three-dimensional temperature and velocity structures of a ME (120 °E) at birth stage, as observed by 12 ~~AUG~~UGs in July 2019 (Figure 1e&6a-b). A warm core was located at subsurface layer and the eddy center exhibited a northeastward vertical tilt (solid black line). In July 2017 (Figures 1c & 6c-d), 10 ~~AUG~~UGs were deployed westward to the Luzon Strait (119 °E). This eddy was in its developing phase and possessed a significant eastward vertical tilt from deep up to surface, reaching depths deeper than 500 m. The eastward vertical tilt is suggested to have been induced by the background current, westward propagation of Rossby Waves (e.g., Qiu et al., 2015; Zhang et al., 2016; Li et al., 2019), and advection background temperature gradient (e.g., Bonnici& Billant, 2020; Gaube et al., 2015; Li, Wang, et al., 2020). Throughout this experiment, the ~~AUG~~UGs encountered the tropical storm "Haitang", results in that the ME underwent horizontal deformation, giving rise to submesoscale processes (Yi et al., 2022; Yi et al., 2024).

In June 2020, 6 ~~AUG~~UGs were deployed across another warm ME in the shelf region (Figures 1g and 6e-h). The eddy was under dissipating stage due to the steep topography, displaying a significant southwestward tilt from a depth of 500 m to surface (Figure 7e-7f). This kind of southwestward vertical tilt was revealed by potential vorticity in a numerical model (Qiu et al., 2022), which was attributed to shallower water depth to the west of mesoscale eddies, and caused asymmetries of the velocities within the MEs. Qiao et al (2023) also captured an eastward movement of a ME by using AUV observations in June 2021(Figure 1h). Based on tensor decomposition of barotropic instability energy, they suggested wave-current interaction played the most important role in the development and propagation of this eddy.

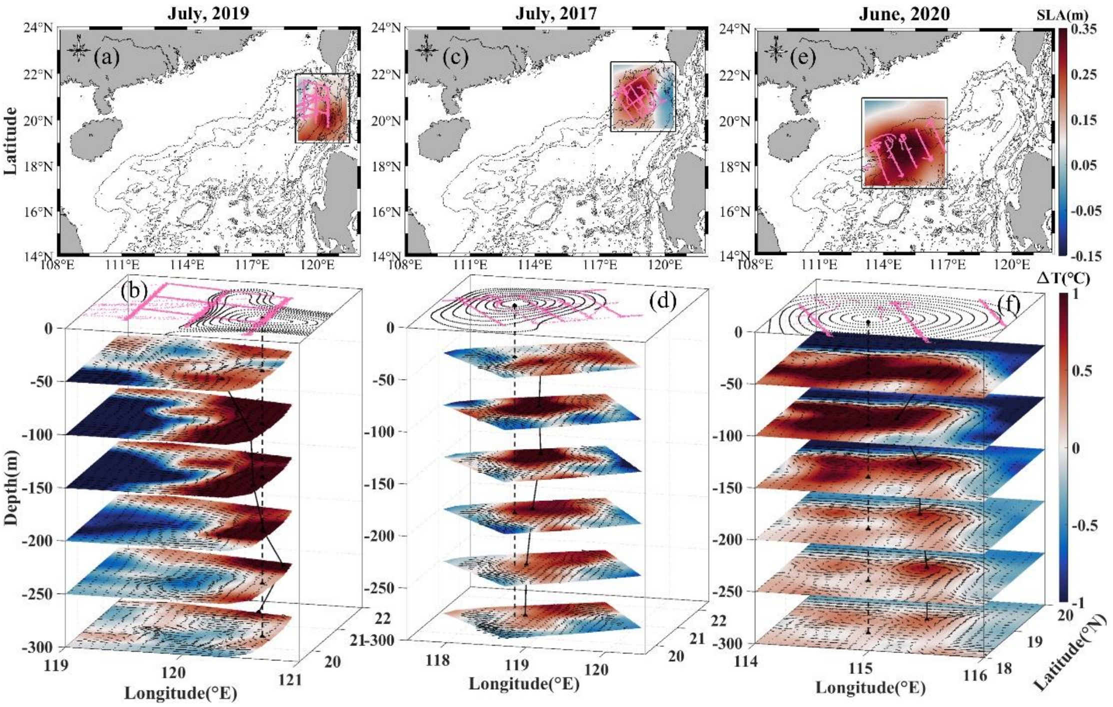

Figure 7. Eddy structures during periods of (a-b) eddy ~~burst~~birth, (c-d) westward movement, and (e-f) dissipation along slope movements. Sea level anomaly (SLA) and ~~AUG~~UGs' positions are superimposed in upper panels (a, c, e), isobaths are represented by solid lines. The ~~AUG~~UG observed temperature and derived geostrophic velocities are in the 3D plots (b, d, f). Pink lines are the tracks of ~~AUG~~UGs. Dashed lines denote the centers of mesoscale eddies from SLA fields, and solid dot lines are the centers from warm cores. UG: Underwater Glider.

4.3 Submesoscale instabilities at the edge of MEs observed by ~~AUG~~UGs

Fine structures, i.e., submesoscale process, usually occurs within MEs, either at the eddy edge (front; filament) or entrained in the eddy center, in terms of spiral structures or "eye-cat" structures (Zhang and Qiu, 2018; Ni et al., 2021; Hu et al., 2023; Qiu et al., 2024). They could cascade kinetic energy downward to turbulent scale via symmetric or centrifugal instabilities, and also induce kinetic energy inverse cascade to MEs via mixed layer baroclinic instabilities (i.e., Fox-Kemper et al., 2008; McWilliams, 2016). However, the submesoscale processes within MEs are difficult to be observed by Argo with 10-day's temporal resolution. Tang et al. (2022) attempted to observe submesoscale fronts using NAVIS float, and found that mixed-layer baroclinic instability dominated this frontogenesis. Qiu et al. (2019) and Shang et al (2023) have captured the submesoscale front at the eddy's edge by using a "virtual mooring" ~~AUG~~UG observation. As passively driven by flow, NAVIS can only observe submesoscale process in an approximate Lagrangian fashion, whereas ~~AUG~~UGs traversing a front could provide us both the cross-front and along-front information, depending on our observational scheme.

In our datasets, 40% of ~~AUG~~UG observations have high spatiotemporal resolutions (<3 km, <4 h; Figure 2), which are fine enough to capture the submesoscale processes positively. Here, we present two examples of submesoscale instabilities at the edge of MEs to show the advantages of ~~AUG~~UG observations.

As shown in Figure 8a, 4 diving ~~AUG~~UGs were deployed at the eddy's edge (front) in 2017. 3 ~~AUG~~UGs cross the front and 1 ~~AUG~~UG tracks along the front. All of them successfully observed the submesoscale instabilities. Following Thomas *et al* (2013), the converted angle of the Richardson number, ϕ_{Ri}, can also be used to determine the nature of the instability:

$$\phi_{Ri} = tan^{-1}\left(-\frac{1}{Ri}\right) = tan^{-1}\left(\frac{|\nabla\cdot b|^2}{N^2\cdot f^2}\right), \qquad (3a)$$

$$Ri \approx Ri_g = \frac{N^2}{\left(\frac{\partial v_g}{\partial z}\right)^2} = \frac{N^2\cdot f^2}{|\nabla\cdot b|^2} < \frac{f}{\zeta_g}, \text{ and } f\cdot\zeta_g > 0. \qquad (3b)$$

where f is the Coriolis parameter, and $\vec{v}_g$ is the geostrophic velocity. $b = -g\rho/\rho_0$, is the buoyancy flux, g is the gravitational acceleration, and ρ is the seawater density, and ρ_0 is the reference density. $N^2 = \partial b/\partial z$ is the vertical buoyancy frequency. $\zeta_g = curl(\overrightarrow{v_g})$ is the vertical relative vorticity. ϕ_{Ri} can be used to judge when instability occurs. For anticyclonic eddies, inertial instability or symmetric instability occurs when $-45° < \phi_{Ri} < \phi_c$; symmetric instability occurs when $-90° < \phi_{Ri} < -45°$; symmetry instability or gravitational instability occurs when $-135° < \phi_{Ri} < -90°$; and gravitational instability occurs when $-180° < \phi_{Ri} < -135°$.

Figure 8a shows that ~~AUG~~UGs observed several types of submesoscale instabilities, in terms of gravity instability, symmetric instability and mixed instabilities from symmetric and centrifugal instabilities at the anticyclonic eddy's edge. Figure 8b shows submesoscale instabilities in 2019. In this case, gravity instability dominates the upper mixed layer. Symmetric and centrifugal instabilities are not significant. These two cases provide us enough information to detect frontal genesis processes in Euler filed, while Navis or Argos provide frontal information in Lagrange view.

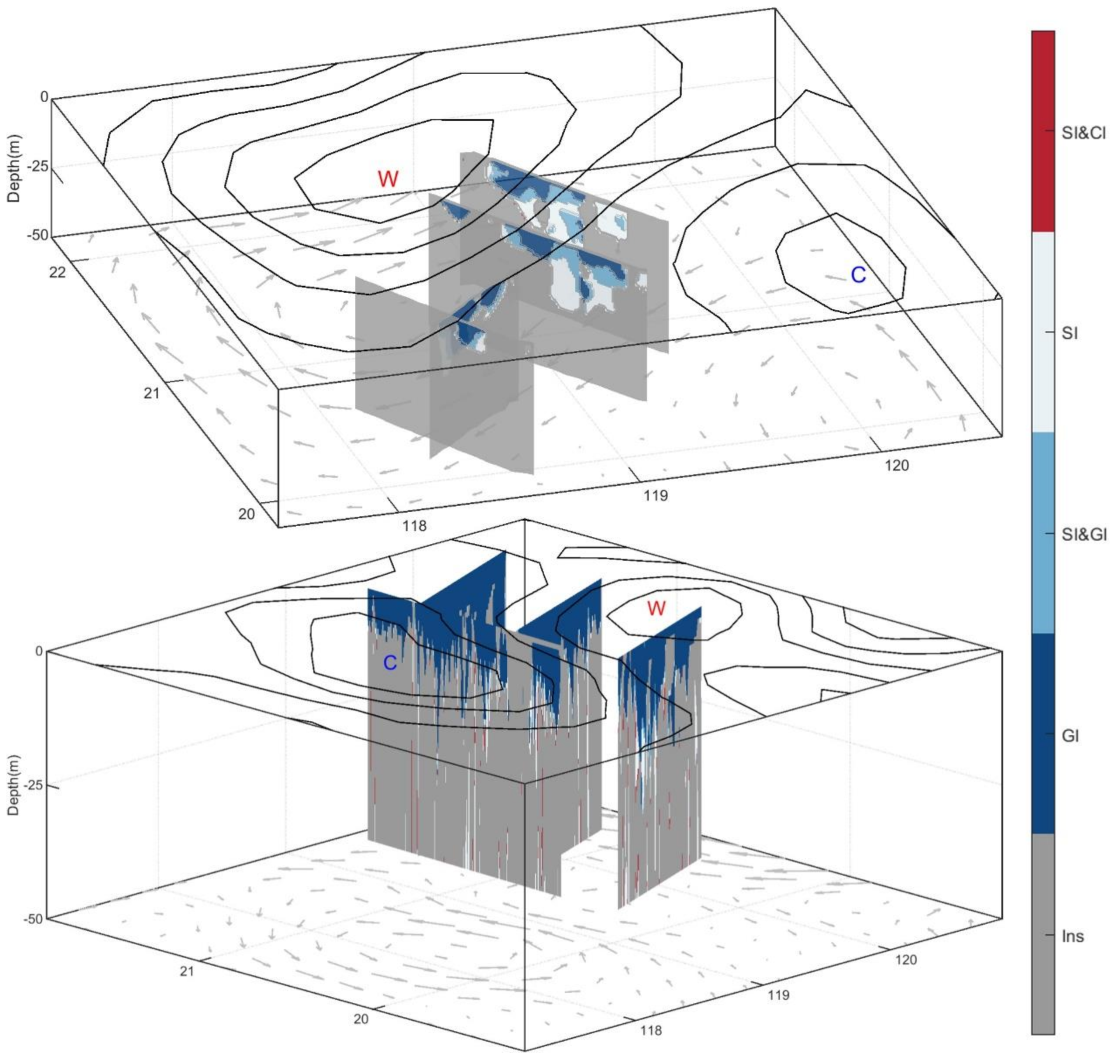

Figure 8. Analyzed submesoscale instabilities at the edge of mesoscale eddies. (a)in 2017, and (b) in 2019. SI: symmetric instability; CI: centrifugal instability; GI: gravity instability. W: anticyclonic eddy; C: cyclonic eddy. Isolines are the sea level anomaly.

5. Data availability

The dataset of AUV and ~~AUG~~UG used in this manuscript was deposited in Science Data Bank, whose DOI is https://doi.org/10.57760/sciencedb.11996 (Qiu et al., 2024b).

6. Conclusions and Potential Future Plan

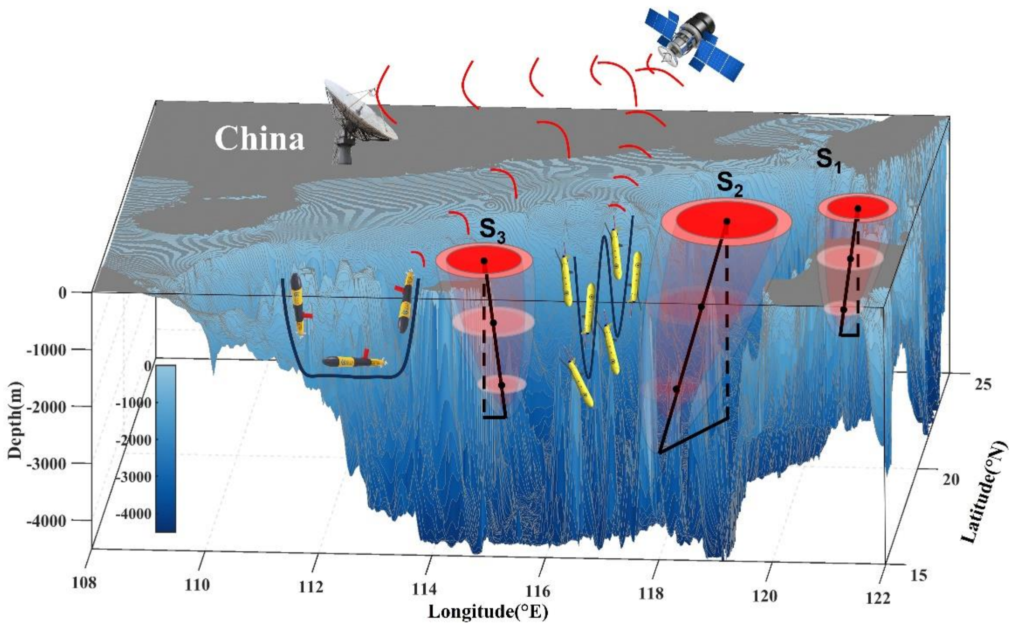

Figure 9. Scheme of ~~AUG~~UGs observed mesoscale eddies at different life stages in the northern SCS. S1: birth stage; S2: developing/mature stage; S3: dissipating stage. UG: Underwater Glider; SCS: South China Sea.

Based on 9-year AUVs and ~~AUG~~UGs observations in SCS, we obtained high-resolution temperature and salinity profiles datasets in SCS. The dataset provides 24498 profiles and covers 463 days' experiments, including 11 experiments from 50 ~~AUG~~UGs and 2 AUVs. To our knowledge, the 9-year dataset is enough in detecting the horizontal asymmetry, vertical tilt, temporal evolution, life cycle of MEs (Figure 9), and the associated submesoscale processes. The dataset supports us to investigate the subsurface MEs, revealing eddy-current and eddy-topography interactions successfully. However, to understand the feedback of MEs to the variability of larger scale current, i.e. western boundary current, routine ~~AUG~~UGs and AUVs observations are needed in future.

Besides tracking MEs, ~~AUG~~UGs and AUVs have been proved to positively capture more smaller scale oceanic process, such as internal tide (Gao et al., 2024), turbulences by using turbulent parameterization schemes (Qi et al, 2020). And ~~AUG~~UGs/AUV installed with more sensors could also provide us geochemical parameters (e.g., Yi et al., 2022), presenting the potential ability in improving the forecast accuracy in physical and biogeochemical numerical model. More projects gathering AUVs network are ongoing and will be promoted in future.

During the mission, we met some challenges: (1) under strong background current, UGs and AUVs get disturbed and cannot follow the customized routes; (2) Under bad weather, the it's difficult for piloting team to deploy and recovery UGs and AUVs; (3) data receiving capacity depends on the satellite transmission capacity. If both the bio-chemistry and CTD data are included, the data resolution have to be lowered. These challenges require piloting team and oceanographers to work together.

Author contributions

Conceptualization: DX~~, JC~~; data curation: CH, ZY, ~~HB,~~ ZH, ~~HB,~~ JW~~, YQ~~; formal analysis: CH, ZY; funding acquisition: CH, DX~~, JC~~; investigation: CH, DX~~, JC~~; methodology: CH, DX~~, JC~~; project administration: CH, DX~~, JC~~; software: CH, DX; supervision: CH, DX; validation: XM, DX, WB; writing: CH, XM. All the authors have read and agreed to the published version of the manuscript.

Financial support

This study was supported by the National Natural Science Foundation of China (Grant No. 42376011; 41976002), National Key R&D Plan Program (No.2017YFC0305804).

Competing interests

The contact author has declared that none of the authors has any competing interests.

Acknowledgements

We acknowledge all the colleagues and project members who have contributed to the design of ~~AUG~~UGs and AUVs, the sea experiments and data processing in the past. Many scientists and engineers have participated in active surveys and mappings. Their work provided basic high-quality materials.

Disclaimer

Publisher's note: Copernicus Publications remains neutral with regard to jurisdictional claims made in the text, published maps, institutional affiliations, or any other geographical representation in this paper. While Copernicus Publications makes every effort to include appropriate place names, the final responsibility lies with the authors.

References:

Bachmayer, R., Leonard, N. E., Graver, J., Fiorelli, E., Bhatta, P. and Paley, D. Underwater glider: Recent developments and future applications, *Proceedings of the 2004 International Symposium on Underwater Technology*, 2004, 195~200. https://doi.org/10.1109/UT.2004.1405540.

Caffaz, A., Caiti, A., Casalino, G. and Turetta, A. The hybrid glider/AUV folaga, *IEEE Robotics and Automation Society*, 2010, 17(1), 31~44. https://doi.org/10.1109/MRA.2010.935791.

Cao, Y., Dong, C., Stegner, A., Bethel, B. J., Li, C., Dong, J., et al. (2023). Global sea surface cyclogeostrophic currents derived from satellite altimetry data. *Journal of Geophysical Research: Oceans*, 128, e2022JC019357. https://doi.org/10.1029/2022JC01935

Chen, G., Hou, Y., Chu, X. Mesoscale eddies in the South China Sea: Mean properties, spatiotemporal variability, and impact on thermohaline structure. *Journal of Geophysical Research-Oceans*, 2011, 116, C06018. https://doi.org/10.1029/2010JC006716

Chelton, D., Schlax, M., Samelson, R., de Szoeke, R. Global observations of large oceanic eddies. *Geophysical Research Letters*, 2007, *34*(15), L15606. https://doi.org/10.1029/2007GL030812

Chelton, D., Schlax, M., Samelson, R. Global observations of nonlinear mesoscale eddies. *Progress in Oceanography*, 2011, 91 (2): 167–216, doi:10.1016/j.pocean.2011.01.002.

Chu, P., Chen, Y., Lu, S. Wind-driven South China Sea deep basin warm-core/cool-core eddies. *Journal of Oceanography*, 1998, 54(4), 347-360. doi: 10.1007/bf02742619.

Chu, P., Fan, C. Optimal linear fitting for objective determination of ocean mixed layer depth from glider profiles. *Journal of Atmospheric and Oceanic Technology*, 2010, 27, 1893–1898.

Dale, W. Winds and drift currents in the South China Sea. *Malayan Journal of Tropical Geography*, 1956, 8, 1-31.

Dong, C., Mcwilliams, J., C., Liu, Y., Chen D. Global heat and salt transports by eddy movement. *Nature Communications*, 2014, 5(2), 3294.

Dong, J., Zhong, Y. The spatiotemporal features of submesoscale processes in the northeastern South China Sea. *Acta Oceanology Sinica*, 2018, 37(11), 8-18. https://doi.org/10.1007/s13131-018-1277-2.

Eriksen, C. C., Osse, T. J., Light, R. D., Wen, T., Lehmann, T. W., Sabin, P. L., Ballard, J. W. and Chiodi, A. M. Seaglider: A long range autonomous underwater vehicle for oceanographic research, *IEEE Journal of Oceanic Engineering*, 2001, 26(4), 424~436. https://doi.org/10.1109/48.972073.

Fang, W., Fang, G., Shi, P., Huang, Q., Xie, Q. Seasonal structures of upper layer circulation in the southern South China Sea from in situ observations. *Journal of Geophysical Research: Oceans*, 2002, 107(C11), 23-1-23-2. doi: 10.1029/2002JC001343.

Fox-Kemper, B., Ferrari, R., Hallberg, R. Parameterization of mixed layer eddies. Part I: Theory and diagnosis. *Journal of Physical Oceanography*, 2008, 38(6), 1145-1165. https://doi.org/10.1175/2007JPO3792.1

Gao, Z., Chen, Z., Huang, X., Yang, H., Wang, Y., Ma, W., & Luo, C. (2024). Estimating the energy flux of internal tides in the northern South China Sea using underwater gliders. *Journal of Geophysical Research: Oceans*, 129, e2023JC020385. https://doi.org/10.1029/ 2023JC020385

He, Q., Zhan, H., Cai, S., He, Y., Huang, G., Zhan, W. A new assessment of mesoscale eddies in the South China Sea: surface features, three-dimensional structures, and thermohaline transports. *Journal of Geophysical Research: Oceans*, 2018, 123(7), 4906-4929.

https://doi.org/10.1029/2018JC014054

He, Q., Zhan, H., Xu, J., Cai, S., Zhan, W., Zhou, L., Zha, G. Eddy-induced chlorophyll anomalies inthe western South China Sea. *Journal of Geophysical Research: Oceans*, 2019, 124, https://doi.org/10.1029/2019JC015371.

He, Y., Xie, J., Cai, S. Interannual variability of winter eddy patterns in the eastern South China Sea. *Geophysical Research Letters*, 2016, 43(10), 5185-5193. doi: 10.1002/2016GL068842.

Hobson, B. W., Bellingham, J. G., Kieft, B., McEwen, R., Godin, M. and Zhang, Y. Tethys-class long range AUVs - extending the endurance of propeller-driven cruising AUVs from days to weeks. *2012 IEEE/OES Autonomous Underwater Vehicles (AUV)*, 2012, 1-8, https://doi.org/10.1109/AUV.2012.6380735.

Hu, Z., Lin, H., Liu Z., Cao Z., Zhang F., Jiang Z., Zhang Y., Zhou K., and Dai M. Observations of a filamentous intrusion and vigorous submesoscale turbulence within a cyclonic mesoscale eddy, *Journal of Physical Oceanography*, 2023, 53(6), 1615–1627.

Huang, Y., Qiao, J., Yu, J., Wang, Z., Xie, Z., Liu, K. Sea-Whale 2000: a long-range hybrid autonomous underwater vehicle for ocean observations. *OCEANS 2019 - Marseille*, Marseille, France, 2019, 1-6, doi: 10.1109/OCEANSE.2019.8867050.

Hwang, C., Chen, S. Circulations and eddies over the South China Sea derived from TOPEX/Poseidon altimetry. *Journal of Geophysical Research: Oceans*, 2000, 105(C10), 23943-23965. doi: 10.1029/2000JC900092.

Li, H., Xu, F., Wang, G. Global mapping of mesoscale eddy vertical tilt. *Journal of Geophysical Research: Oceans*, 2022, 127, e2022JC019131. https://doi.org/10.1029/2022JC019131

Li, L., Worth. D., Nowlin, J., Su. J. Anticyclonic rings from the Kuroshio in the South China Sea. *Deep Sea Research Part I*, 1998, 45, 1469-1482. doi: 10.1016/s0967-0637(98)00026-0.

Lin, X., Dong, C., Chen, D., Liu, Y., Yang, J., Zou, B., Guan, Y. Three-dimensional properties of mesoscale eddies in the South China Sea based on eddy-resolving model output. *Deep-Sea Research Part I: Oceanographic Research Papers*, 2015, 99, 46-64. https://doi.org/10.1016/j.dsr.2015.01.007

Lin, P., Wang, F., Chen, Y., & Tang, X. Temporal and spatial variation characteristics of eddies in the South China Sea I: Statistical analyses. Acta Oceanologica Sinica,2007, 29(3), 14-22.

McWilliams, J. Submesoscale currents in the ocean. *Proceedings of the Royal Society A,* 2016, 472, 20160117. http://dx.doi.org/10.1098/rspa.2016.0117

Morison, J., Andersen, R., Larson, N., D'Asaro, E., Boyd, T. The correction for thermal-lag effects in Sea-Bird CTD data. *Journal of Atmospheric and Oceanic Technology*, 1994, 11, 1151–1164, https://doi. org/10.1175/1520-0426(1994)011,1151:TCFTLE.2.0.CO;2.

Morrow, R., Birol, F., Griffin, D., Sudre, J. Divergent pathways of cyclonic and anti-cyclonic ocean eddies. *Geophysical Research Letters*, 2004, *31*(24), L24311. https://doi.org/10.1029/2004gl020974

Nan, F., He, Z., Zhou, H., Wang, D. Three long-lived anticyclonic eddies in the northern South China Sea. *Journal of Geophysical Research: Oceans*, 2011, 116(5), C05002. https://doi.org/10.1029/2010JC006790

Ni, Q., Zhai, X., Wilson, C., Chen, C., Chen, D. Submesoscale eddies in the South China Sea. *Geophysical Research Letters*, 2021, 48, e2020GL091555. https://doi.org/10.1029/2020GL091555

Oey, L. Eddy- and wind-forced shelf circulation. *Journal of Geophysical Research*, 1995, *100*(C5), 8621–8637.https://doi.org/10.1029/95JC00785.

Okkonen, S., Weingartener, T., Danielson, S., Musgrave, D., Schmidt, G. M. Satellite and hydrographic observations of eddy-induced shelf-slope exchange in the northwestern Gulf of Alaska. *Journal of Geophysical Research*, 2003, *108*(C2), 3033. https://doi.org/10.1029/2002JC001342.

Osse, T. J. and Eriksen, C. C. The deepglider: a full ocean depth glider for oceanographic research. *OCEANS 2007*, 2007, 1~12. https://doi.org/10.1109/OCEANS.2007.4449125.

Qi, Y., Shang, C., Mao, H., Qiu, C., Shang, X. Spatial structure of turbulent mixing of an anticyclonic mesoscale eddy in the northern South China Sea. *Acta Oceanologica Sinica*, 2020, 39(11), 69-81. https://doi.org/10.1007/s13131-020-1676-z.

Qiao, J., Qiu, C., Wang, D., Huang, Y., Zhang, X., Huang, Y. Multi-stage Development within Anisotropy Insight of an Anticyclone Eddy Northwestern South China Sea in 2021. *Geophysical Research Letter*, 2023, doi:10.1029/2023GL104736

Qiu, C., Mao, H., Yu, J., Xie, Q., Wu, J., Lian, S., Liu, Q. Sea surface cooling in the Northern South China Sea observed using Chinese Sea-wing Underwater Glider Measurements. *Deep Sea Research Part I: Oceanographic Research Papers*, 2015, 105, 111-118.

Qiu, C., Mao, H., Liu, H., Xie, Q., Yu, J., Su, D., Ouyang, J., Lian, S. Deformation of a warm eddy in the northern South China Sea. *Journal of Geophysical Research: Oceans*, 2019, 124, 5551-5564. https://doi.org/10.1029/2019JC015288

Qiu, C., Mao, H., Wang, Y., Su, D., Lian, S. An irregularly shaped warm eddy observed by Chinese underwater gliders. *Journal of Oceanography*, 2019, 75, 139-148.

Qiu, C., Liang, H., Huang, Y., Mao, H., Yu, J., Wang, D., Su, D. Development of double cyclonic mesoscale eddies at around Xisha Islands observed by a 'Sea-Whale 2000' autonomous underwater vehicle. *Applied Ocean Research*, 2020, https://doi.org/10.1016/j.apor.2020.102270.

Qiu, C., Yi, Z., Su, D., Wu, Z., Liu, H., Lin, P., He, Y., Wang, D. Cross-slope heat and salt transport induced by slope intrusion eddy's horizontal asymmetry in the northern South China Sea. *Journal of Geophysical Research: Oceans,* 2022, doi: 10.1029/2022JC018406.

Qiu, C., Yang, Z., Feng, M., Yang, J., Rippeth, T.P., Shang, X., Sun, Z., Jing, C., Wang, D. Observational energy transfers of a spiral cold filament within an anticyclonic eddy. *Progress in Oceanography*, 2024a, https://doi.org/10.1016/j.pocean.2023.103187**.**

Qiu, C., Du, Z., Yu, J., et al. ~~AUG~~UG and AUV data used in research "A High Dense Temperature-Salinity Dataset Observed by ~~Automatic~~Autonomous Underwater Vehicles toward Mesoscale eddies' Evolutions and Associated Submesoscale Processes in South China Sea" [DS/OL]. V2. Science Data Bank, 2024b[2024-08-03]. https://doi.org/10.57760/sciencedb.11996. DOI: 10.57760/sciencedb.11996.

Rainville, L., Lee, C., Arulananthan, K., Jinadasa, S., Fernando, H., Priyadarshani, W., Wijesekera, H. Water mass exchanges between the Bay of Bengal and Arabian Sea from multiyear sampling with autonomous gliders. *Journal of Physical Oceanography*, 2022, 52, 2377–2396, https://doi.org/10.1175/JPO-D-21-0279.1.

Shang, X., Shu, Y., Wang, D., Yu, J., Mao, H., Liu, D., Qiu, C., Tang, H. Submesoscale motions driven by down-front wind around an anticyclonic eddy with a cold core. *Journal of Geophysical Research: Oceans*, 2023, 128, e2022JC019173. https://doi.org/10.1029/2022JC019173.

Sherman, J., Davis, R. E., Owens, W. B. and Valdes, J., 2001. The autonomous underwater glider “Spray”, IEEE J. Ocean Eng., 26(4): 437~446.

Shu, Y., Xiu, P., Xue, H., Yao, J., Yu, J. (2016). Glider-observed anticyclonic eddy in northern South China Sea. *Aquatic Ecosystem Health & Managemen*t, 19(3), 233–241. https://doi.org/10.1080/14634988.2016.1208028

Su, D., Lin, P., Mao, H., Wu, J., Liu, H., Cui, Y., Qiu, C. Features of slope intrusion mesoscale eddies in the northern South China Sea. *Journal of Geophysical Research: Oceans,* 2020, 125, e2019JC015349. https://doi.org/ 10.1029/2019JC015349.

Tang, H., Shu, Y., Wang, D., Xie, Q., Zhang, Z., Li, J., Shang, X., Zhang, O., Liu, D. Submesoscale processes observed by high-frequency float in the western South China Sea. *Deep Sea Research Part I: Oceanographic Research Papers*, 2022, 103896. https://doi.org/10.1016/j.dsr.2022.103896

Thomas, L., Taylor, J., Ferrari, R., Terrence M. Symmetric instability in the Gulf Stream. *Deep Sea Research Part II: Topical Studies in Oceanography*, 2013, 91, 96-110. https://doi.org/10.1016/j.dsr2.2013.02.025

Todd, R.E., Ren, A.S. Warming and lateral shift of the Gulf Stream from in situ observations since 2001. *Nature Climate Change,* 2023, **13**, 1348–1352. https://doi.org/10.1038/s41558-023-01835-w

Wang, G., Su, J., Chu, P. Mesoscale eddies in the South China Sea observed with altimetry. *Geophysical Research Letter*, 2003, 30(21), 2121. doi: 10.1029/2003GL018532.

Wang, G., Chen, D., Su, J. Winter eddy genesis in the eastern South China Sea due to orographic wind jets. *Journal of Physical Oceanography*, 2008, 38(3), 726–732. https://doi.org/10.1175/2007jpo3868.1

Wang, Q., Zeng, L., Li, J., Chen, J., He, Y., Yao, J., Wang, D., Zhou, W. Observed Cross-Shelf Flow Induced by Mesoscale Eddies in the Northern South China Sea. *Journal of Physical Oceanography*, 2018, 48, 1609–1628. https://doi.org/10.1175/JPO-D-17-0180.1

Wang, D., Xu, H., Lin, J., Hu, J. Anticyclonic eddies in the northeastern South China Sea during winter of 2003/2004. *Journal of Oceanography*, 2008, 64(6), 925-935

Wang, Z., Chen, Q. Warm core eddies in the northern South China Sea (I): Preliminary observations of warm eddies in the South China Sea. J*ournal of Oceanography of Taiwan Strait*,1987, 18, 92-103.

Xu, J., Su, J. Hydrographic analysis of Kuroshio intrusion into the South China Sea II: Observations during AugUGust-September 1994. *Tropical Oceanography*,1997, 2, 1-23.

Yang, H., Liu, Q. The seasonal features of temperature distributions in the upper layer of the South China Sea. *Oceanologia et Limnologia Sinica*, 1998,29(5), 501-507.

Xiu, P., Chai, F., Shi, L., Xue, H., Chao, Y. A census of eddy activities in the South China Sea during 1993-2007. *Journal of Geophysical Research: Oceans*, 2010,115, C03012. doi: 10.1029/2009JC005657.

Yang, Q., Nikurashin, M., Sasaki, H., Sun, H., Tian, J. Dissipation of mesoscale eddies and its contribution to mixing in the northern South China Sea. *Scientific Reports*, 2019, 9. https://doi.org/10.1038/s41598-018-36610-x

Yi, Z., Wang, D., Qiu, C., Mao, H., Yu, J., Lian, S. Variations in dissolved oxygen induced by a tropical storm within an anticyclone in the Northern South China Sea. *Journal of Ocean University of China*, 2022, 21(5), 1084-1098. https://doi.org/10.1007/s11802-022-4992-4.

Zhang, Z., Qiu, B. Evolution of submesoscale ageostrophic motions through the life cycle of oceanic mesoscale eddies. *Geophysical Research Letters,* 2018, 45(21), 11847-11855. https://doi.org/10.1029/2018GL080399

Zhang, Z., Tian, J., Qiu, B., Zhao, W., Chang, P., Wu, D. Observed 3D Structure, Generation, and Dissipation of Oceanic Mesoscale Eddies in the South China Sea. *Scientific Reports,* 2016, 6(1), 24349. https://doi.org/10.1038/srep24349

Zhang, Z., Zhao, W., Qiu, B., Tian, J. Anticyclonic eddy sheddings from Kuroshio loop and the accompanying cyclonic eddy in the Northeastern South China Sea. *Journal of Physical Oceanography*, 2017, 47(6), 1243-1259. https://doi.org/10.1175/JPO-D-16-0185.1